Acta Mech 230, 2111–2123 (2019)
https://doi.org/10.1007/s00707-019-2371-z

ORIGINAL PAPER

Xiaolong Li · Xiaoqian Chen · Yiyong Huang · Xiang Zhang

Effect of interface wettability on the flow characteristics of liquid in smooth microchannels

Received: 6 July 2018 / Revised: 10 January 2019 / Published online: 14 March 2019

Abstract Rapid advances in microfluidic devices have induced interest in the study of the microscale flow mechanism. However, the experimental results of microscale flow often deviate from the classical theory, and we attribute this deviation to the changing liquid viscosity in the microchannels. Because of the effect of the solid–liquid intermolecular force, the viscosity of the liquid near the walls is different from the bulk viscosity. Based on molecular theory and wetting theory, we propose a modified apparent viscosity model. The apparent viscosity of the liquid in microchannels increases with the increase in wettability and decreases with the increase in distance from the wall and the increase in drive pressure. The apparent viscosity near the hydrophilic wall is higher than the bulk viscosity, which increases the flow friction in the microchannels. To validate this model, we experimentally investigate the frictional characteristic of a deionized water flow in smooth parallel-plate microchannels with different wettabilities and heights of approximately 20 and 50 μm. The results indicate that the friction factor is higher than that predicted by the classical theory. Such a difference increases with increasing wettability and decreases with increasing hydraulic diameter and pressure drop, which is consistent with the results of theoretical analysis. The apparent viscosity calculated by the apparent viscosity model notably fit the experimental results, with a relative difference of less than ±2.1%.

List of symbols

A_{ch}	Cross-sectional area of the channel (m^2)
A_p	Cross-sectional area of the plenum (m^2)
D_h	Hydraulic diameter (μm)
F_{LL}	Liquid–liquid intermolecular forces (N)
F_{LS}	Solid–liquid intermolecular forces (N)
f	Darcy's friction factor
H	Height of the microchannel (μm)
K_{90}	Bend loss coefficient
K_c	Contraction loss coefficient
K_e	Expansion loss coefficient
k	Coefficient in Eq. (3)
L	Length of the microchannel (mm)
n	Coefficient in Eq. (3)
ΔP	Frictional pressure drop (Pa)
ΔP_{H1}	Inlet hydrostatic pressure losses (Pa)
ΔP_{H2}	Outlet hydrostatic pressure losses (Pa)

X. Li · X. Chen (✉) · Y. Huang · X. Zhang
College of Aerospace Science and Engineering, National University of Defense Technology, Changsha 410073, Hunan, China
E-mail: chenxiaoqian@nudt.edu.cn

P_{in}	Inlet pressure (Pa)
P_{out}	Outlet pressure (Pa)
u	Velocity in the x-direction (m/s)
u_{m}	Mean velocity (m/s)
Re	Reynolds number
W	width of the microchannel (mm)
x, y	Cartesian coordinates (m)
δ	Mean distance between two adjacent molecules (nm)
μ_0	Bulk viscosity [kg/(m s)]
μ_{a}	Apparent viscosity [kg/(m s)]
$\bar{\mu}_{\text{a}}$	Average apparent viscosity [kg/(m s)]
θ	Contact angle (°)
ρ	Density (kg/m^3)
σ_{L}	Surface tension of the liquid (N/m)
σ_{L}^0	Internal surface force of the liquid (N/m)
σ_{LS}	Interfacial tension of the liquid (N/m)
σ_{LS}^0	External surface force of the liquid (N/m)
ξ	Parameter in Eq. (2)

Subscripts

exp	Experimental value
th	Theoretical value
1	Value of the top wall
2	Value of the bottom wall

1 Introduction

With the rapid development of micromachining technology, the characteristic scales of the channel in microfluidic devices decrease to micro- and nanoscales. Broad applications of microfluidic devices require the accurate prediction of liquid flows in microchannels, which has attracted many researchers in various fields to study the microflow mechanism [1,2]. However, the experimental results of liquid flows in microchannels often deviate from the predictions of the classical flow theory, and the deviation commonly increases with a decrease in diameters [3–7].

The frictional characteristic of liquid flows in microchannels is affected by various interfacial factors such as the surface roughness [8–10], boundary slip [11,12], wettability [13,14], and interfacial electric double layer (EDL) [15,16]. Because the influential range of interfacial effects is substantially smaller than the hydraulic diameters of the channel, these interfacial effects are commonly ignored in the macroscale flow. However, the interfacial effects significantly affect the flow when the channel size is decreased to the microscale level. The surface roughness is an important factor that causes the discrepancy between experimental and theoretical results for liquid flows in microchannels. Mala and Li [8] observed that for water flows in microtubes with a surface relative roughness of 0.007–0.035, the friction factors are 14–50% higher than the theoretical values. Based on the experimental data, the authors proposed a roughness-viscosity function to quantify the effect of the surface roughness on the microflow. However, Wang et al. [13] and Xu et al. [17] found that the inconsistencies between experiment and classical theory remain for water flows in smooth microtubes.

The inaccuracy of the classical theory predictions can be clarified by the change in viscosity of the liquid in microchannels. The liquid viscosity is the macro-representation of the intermolecular force: For the liquid molecules near the wall, the forces that act on them are the liquid–liquid intermolecular force, solid–liquid intermolecular force, and electrostatic force [18]. Mala et al. [15,19] found that the electric double layer (EDL) caused by the electrostatic force resulted in a higher apparent viscosity than the bulk value. Even if it is not affected by the EDL, the viscosity measurement experiment shows that the liquid viscosity in notably small spaces can be much higher than that in the bulk region [20,21]; the liquid viscosity in small microcrevices continuously decreases from the solid surface to the bulk and is affected by the solid surface and liquid molecule structure [22]. The molecular dynamic simulations also indicate that the liquid viscosity can be inhomogeneous

near the wall [23–25]. Therefore, the effect of the solid–liquid intermolecular force on the liquid viscosity near the wall is not negligible in microchannels. Considering the effect of the solid–liquid intermolecular force, You et al. [18] derived an apparent viscosity model for the liquid near the wall from the molecular theory. Because the solid–liquid intermolecular force is difficult to directly calculate and the strength of the wettability is determined by the intermolecular force, the effect of the solid–liquid intermolecular force on viscosity and liquid flow in microchannels can be investigated by studying the effect of the interface wettability on that.

In this investigation, the effect of interface wettability on the apparent viscosity and liquid flow in smooth microchannels is discussed. A modified model based on the molecular theory and wetting theory is proposed by considering the relationship between interface wettability and intermolecular forces. Moreover, an experiment system is designed and implemented to investigate the frictional characteristic of deionized water flows in smooth parallel-plate microchannels. Finally, the modified apparent viscosity model is verified using experimental results.

2 Modified model based on molecular theory and wetting theory

The parallel-plate Poiseuille flow under the no-slip boundary condition in Fig. 1 shows that the velocity distribution of a fully developed laminar flow can be derived from the continuity and Navier–Stokes equations:

$$u(y) = \frac{\mathrm{d}P}{\mathrm{d}x} \int \frac{y}{\mu_\mathrm{a}} \mathrm{d}y + C \tag{1}$$

where u is the velocity in the x direction, $-(\mathrm{d}P/\mathrm{d}x)$ is the pressure gradient, μ_a is the liquid viscosity, and C is the constant of integration.

Equation (1) shows that the change in liquid viscosity directly affects the flow behavior. In the classical theory, the liquid viscosity is considered a position-independent constant. However, the liquid viscosity is a variable related to the distance from the wall if the effect of solid–liquid interaction is present [18]. Because the liquid viscosity is related to the strength of the intermolecular force, the liquid viscosity near the wall consists of two parts: the viscosity generated by the liquid–liquid intermolecular force, which is identical to the bulk viscosity, and the additional viscosity generated by the solid–liquid intermolecular force, which decreases with the increase in distance from the wall and is commonly ignored for macroflows. When the characteristic dimension of the flow is comparable to the influential length of the solid–liquid intermolecular force, the effects of the variable viscosity on the microflow cannot be ignored. To understand the effect of the variable viscosity on the microflow, the viscosity model of the liquid near the wall should be established.

Based on the molecular theory, You et al. [18] proposed an apparent viscosity model for liquids between two parallel plates

$$\mu_\mathrm{a} = \mu_0 + \frac{\xi_1}{(H/2 - y)^{n_1}} + \frac{\xi_2}{(H/2 + y)^{n_2}} \tag{2}$$

where μ_a is the apparent viscosity; μ_0 is the bulk viscosity; ξ is the solid–liquid intermolecular interaction; n is the decay rate of the solid–liquid intermolecular interaction with respect to the distance from the wall; indices 1 and 2 indicate the value at the top and bottom walls, respectively; and H is the spacing between the parallel plates.

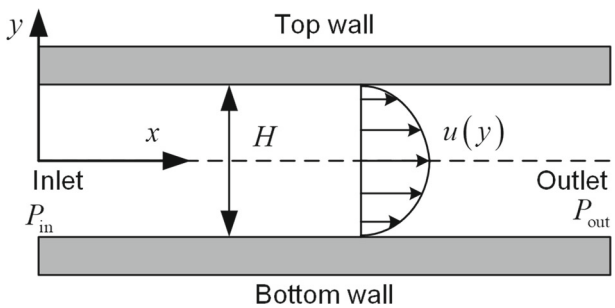

Fig. 1 Parallel-plate Poiseuille flow in the no-slip boundary condition

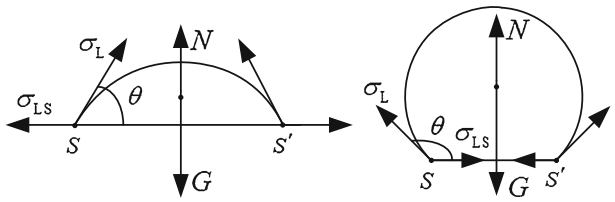

Fig. 2 Schematic of the contact angle in the interface layer model of the physical interface: **a** wetting; **b** non-wetting

However, the value of ξ is difficult to calculate directly. Assuming that the viscosity is proportional to the magnitude of the intermolecular force, ξ can be replaced by $k\mu_0$, then the apparent viscosity model can be improved as follows:

$$\mu_a = \mu_0 + k_1\mu_0\left(\frac{\delta}{H/2-y}\right)^{n_1} + k_2\mu_0\left(\frac{\delta}{H/2+y}\right)^{n_2},\ y \in \left[-\frac{H}{2}+\delta, \frac{H}{2}-\delta\right], \tag{3}$$

$$k_1 = \frac{\left|F_{LS_1}\right| - F_{LL}}{F_{LL}},\ k_2 = \frac{\left|F_{LS_2}\right| - F_{LL}}{F_{LL}} \tag{4}$$

where δ is the mean distance between two adjacent molecules and is approximately equal to the molecular diameter; k is determined by the intermolecular forces; and F_{LS} and F_{LL} are the intermolecular forces that act on the liquid molecules with a distance of δ from the wall by the solid molecules and other liquid molecules, respectively. The directions of F_{LS} and F_{LL} are perpendicular to the solid–liquid interface and are opposite, and assuming that the force with the direction pointing to the liquid is in a positive direction, so there are $F_{LS} < 0$ and $F_{LL} > 0$.

Because the intermolecular force is difficult to calculate, the strength of the solid–liquid intermolecular force can commonly be gauged from the static contact angle [26]. According to the interface layer model of the physical interface [27], the internal surface force of the liquid phase σ_L^0 is defined as the necessary work to overcome the liquid–liquid intermolecular force when the surface is increased in unit area, then there is $\sigma_L^0 = F_{LL} > 0$; the external surface force of the liquid phase σ_{LS}^0 is defined as the necessary work to overcome the solid–liquid intermolecular force when the surface increases in unit area, then there is $\sigma_{LS}^0 = F_{LS} < 0$. From the interface layer model, we obtain

$$\sigma_L = \sigma_L^0,\ \sigma_{LS} = \sigma_L^0 + \sigma_{LS}^0 \tag{5}$$

where σ_L and σ_{LS} are the surface tension and interfacial tension of the liquid phase, respectively. Since $\sigma_L^0 > 0$ and $\sigma_{LS}^0 < 0$, σ_L is always positive; when $\left|\sigma_{LS}^0\right| > \sigma_L^0$, $\sigma_{LS} < 0$, when $\left|\sigma_{LS}^0\right| \le \sigma_L^0$, $0 \le \sigma_{LS} < \sigma_L$.

Then, for each wall, we obtain

$$k_{1,2} = -\left(\frac{\sigma_{LS}}{\sigma_L}\right)_{1,2}. \tag{6}$$

When $\sigma_{LS} < 0$, $k_{1,2} > 0$; when $0 \le \sigma_{LS} < \sigma_L$, $k_{1,2} > -1$. Therefore, $k_{1,2}$ is always larger than -1, according to Eq. (3), the viscosity of the liquid is always positive. According to Eq. (6), $k_{1,2}$ can be calculated by the surface tension σ_L and interfacial tension σ_{LS}. Besides, the contact angle θ is related to σ_L and σ_{LS}. Therefore, $k_{1,2}$ can also be calculated by the contact angle.

Unlike Young's equation, the interface layer model of the physical interface considers that the liquid and solid phases should be independently discussed when we discuss the wettability [27]. The schematic of the contact angle in this model is shown in Fig. 2.

When $-\sigma_{LS}^0 > \sigma_L^0$, the liquid phase wets the solid phase, i.e., $\theta < 90°$, especially when $-\sigma_{LS}^0 \ge 2\sigma_L^0$, it can be obtained from Eq. (5) that $|\sigma_{LS}| \ge \sigma_L$, at this time, the liquid phase wets the solid phase completely, $\theta = 0°$. When $-\sigma_{LS}^0 = \sigma_L^0$, it can be obtained from Eq. (5) that $\sigma_{LS} = 0$, which is between wetting and non-wetting, and there is $\theta = 90°$. When $-\sigma_{LS}^0 < \sigma_L^0$, the liquid phase does not wet the solid phase, i.e., $\theta > 90°$, and because the intermolecular forces between two phases must exist, i.e., $\sigma_{LS}^0 \ne 0$ is always valid, from Eq. (5) we get that $\sigma_{LS} < \sigma_L$, so $90° < \theta < 180°$.

When $0° < \theta < 180°$, the wetting equation of the liquid phase can be obtained from the force balance in the horizontal direction at the three-phase contact point,

$$\sigma_{\mathrm{L}} \cos\theta + \sigma_{\mathrm{LS}} = 0. \tag{7}$$

For the case of wetting, $\sigma_{\mathrm{L}} > 0, \sigma_{\mathrm{LS}} < 0$, so $\cos\theta > 0, \theta < 90°$; for the case of non-wetting, $\sigma_{\mathrm{L}} > 0, \sigma_{\mathrm{LS}} > 0$, so $\cos\theta < 0, \theta > 90°$; for the case of $\sigma_{\mathrm{LS}} = 0$, $\cos\theta = 0, \theta = 90°$. All three cases are consistent with the actual situation, so Eq. (7) should be correct.

By substituting Eq. (7) into Eq. (6) and simplifying the result, we obtain

$$k_{1,2} = \cos\theta_{1,2}. \tag{8}$$

When $0° < \theta < 180°$, $k_{1,2}$ can be calculated from both Eqs. (6) and (8). Since the measurement of the contact angle is simpler than that of surface tension and interfacial tension, Eq. (8) is more convenient in application. However, Eq. (8) also has limitations. For the case of complete wetting ($\theta = 0°$), the imbalance of forces in the horizontal direction leads to the failure of Eq. (7), which further makes Eq. (8) invalid. Therefore, $k_{1,2}$ can only be calculated using Eq. (6) when $\theta = 0°$. Equations (3) and (8) show that the apparent viscosity of the liquid in the microchannel increases with the increase in interface wettability but decreases with the increase in distance from the wall. If the solid–liquid intermolecular force and liquid–liquid intermolecular force have equal strengths, then $\theta = 90°$, $k = 0$, and the apparent viscosity is equal to the bulk viscosity.

Parameter $n_{1,2}$ reflects the attenuation degree of the solid–liquid intermolecular force relative to the distance from the wall. You et al. [18] thought that $1 < n < 4$, the influential distance of the solid–liquid intermolecular force will be only several or tens of nanometers. However, Lv et al. [22] found that the viscosities of water and hydrocarbon in microcrevices of several hundred micrometers were significantly higher than the bulk values. This may be due to that in the model of Ref. [18] the effect of the hydrogen bond and arrangement of liquid molecules on the viscosity are not considered. The viscosity of many liquids such as water is significantly affected by the hydrogen bonds among liquid molecules. Thus, the orderly arrangement of liquid molecules strongly affects the viscosity by increasing the number of hydrogen bonds. For example, the viscosity of water significantly increases when its temperature decreases mainly because the arrangement of water molecules tends to be more orderly when the temperature decreases. Because of the attraction of the solid wall, the water molecules near the wall are arranged in an orderly manner, which increases the liquid–liquid intermolecular force and decreases the attenuation degree of the solid–liquid intermolecular force relative to the distance from the wall. n may be less than 1, and the influential distance of the hydrophilic wall can be several or tens of micrometers. n is affected by the properties of the liquid and solid wall and can be experimentally determined.

The average apparent viscosity can be obtained by integrating Eq. (3),

$$\bar{\mu}_{\mathrm{a}} = \mu_0 + \frac{k_1\mu_0}{H}\int_{-\frac{H}{2}+\delta}^{\frac{H}{2}-\delta}\left(\frac{\delta}{H/2-y}\right)^{n_1}\mathrm{d}y + \frac{k_2\mu_0}{H}\int_{-\frac{H}{2}+\delta}^{\frac{H}{2}-\delta}\left(\frac{\delta}{H/2+y}\right)^{n_2}\mathrm{d}y, \quad n_{1,2} > 0. \tag{9}$$

It has been found that slip flow may occur on the hydrophobic surfaces; the stronger the hydrophobicity, the larger the slip length. However, the well-accepted no-slip boundary condition is still applicable for the hydrophilic cases [11,12,28]. In this paper, we focus on the hydrophilic cases and ignore the slip flow. Substituting Eq. (9) into Eq. (1) and integrating Eq. (1), we derive the theoretical mean velocity under the boundary condition of no-slip as follows:

$$u_{\mathrm{m\_th}} = \frac{H^3}{12\bar{\mu}_{\mathrm{a}}}\left(-\frac{\mathrm{d}P}{\mathrm{d}x}\right). \tag{10}$$

Strictly speaking, the theoretical mean velocity should be derived by substituting Eq. (3) into Eq. (1) and averaging after integrating in the y direction. This process is notably complicated and can only be calculated using numerical integration. Here, we simplify the calculation by first calculating the average apparent viscosity.

For $k = 0$ or $H \gg \int_{-H/2+\delta}^{H/2-\delta}\delta^n/(H/2 \mp y)^n\mathrm{d}y$, there is $\bar{\mu}_{\mathrm{a}} = \mu_0$, Eq. (10) is simplified to the classical theory. For liquid flows in microchannels with hydrophilic walls, $k > 0, \bar{\mu}_{\mathrm{a}} > \mu_0$, and the flow velocity is lower than the classical theoretical value, i.e., the liquid in hydrophilic microchannels has a higher flow friction than that predicted by the classical theory. With the trend of the apparent viscosity, the relative difference between the solution of Eq. (10) and the classical theory increases with increasing wettability and decreases with increasing hydraulic diameter and pressure drop.

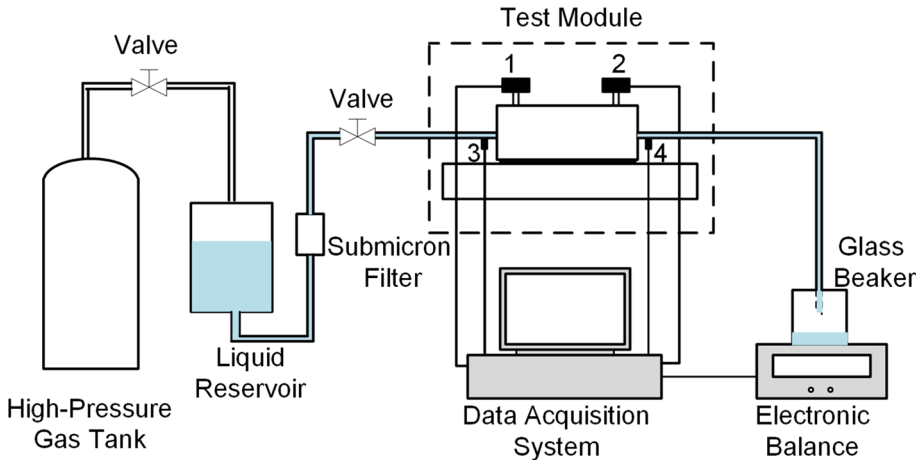

Fig. 3 Schematic of the experimental system: 1, 2 pressure transducer; 3, 4 thermocouple

3 Experiment design and implementation

The viscosity of liquid in the microchannel is difficult to directly measure, but we can obtain the average apparent viscosity from the flow experiment based on the relationship between the viscosity and the mass flow rate. To validate the modified apparent viscosity model, an experiment system is designed and implemented to investigate the flow characteristic of liquid in a smooth parallel-plate microchannel with different wettabilities.

Figure 3 shows the experimental system to study the effect of the wettability on the flow characteristics of liquids in microchannels. The main components of the system are the following: (i) a high-pressure gas tank; (ii) a liquid reservoir; (iii) a submicron filter; (iv) a test module including a microchannel, two pressure transducers, and two thermocouples; (v) an electronic balance with a glass beaker; and (vi) a data acquisition system.

A microchannel plate is placed between a cover plate and a bottom plate to form a test module, as shown in Fig. 4a. Two O-rings between the cover plate and the microchannel plate maintain a leak-proof seal. The microchannels were fabricated by bonding the processed BF-33 glass sheet with the processed silicon plate; the schematics of the microchannel are shown in Fig. 4b, c. To contrast the flow characteristics of the liquid in microchannels with different wettabilities, a thin silver film with a thickness of about 50 nm was deposited on the bottom of some microchannels before the bonding process, whereas the other microchannels were not treated.

The typical cross section images by scanning electron microscopy (SEM) are shown in Fig. 5. The SEM measurements were taken after the flow experiments were completed, and the microchannels used in the flow experiments were cut in the direction of z to a size suitable for SEM measurements. Therefore, the heights of the microchannels used in the flow experiments can be obtained by such SEM images. Figure 5 shows that the surface of the microchannel is notably smooth, so the effect of the surface roughness is negligible.

The dimensions of the microchannels in this work are listed in Table 1. The bottom surface of channels No. 2 and No. 4 is covered by a silver-plated layer, whereas channels No. 1 and No. 3 have no silver-plated layer. Therefore, channels No. 2 and No. 4 have different interface wettabilities from those of channels No. 1 and No. 3.

Deionized water at room temperature was used as the working fluid. To calculate coefficient k in the apparent viscosity model, the static contact angles of different solid–liquid interfaces were measured, and the results are shown in Fig. 6. Figure 6b, c show that the wettability of the microchannels varies: for the silicon–water interface of channels No. 1 and No. 3, $\theta \approx 34°$; and for the silver–water interface of channels No. 2 and No. 4, $\theta \approx 90°$. From Eqs. (9) and (10), the average apparent viscosity of water in channels No. 1 and No. 3 is larger than that in channels No. 2 and No. 4, respectively; thus, the flow rate of the water flow in the silicon-based microchannel is lower than that in the silver-plated microchannel.

In the experiments, the testing liquid was forced to flow through the microchannel by a high-pressure gas. The inlet and outlet pressures of the microchannel were measured separately using two absolute-pressure transducers (BD Sensors, DMP331i) with an accuracy of 0.05%. The liquid temperatures at the inlet and outlet of the microchannel were separately measured using two J-type thermocouples with 1 °C accuracy, and the

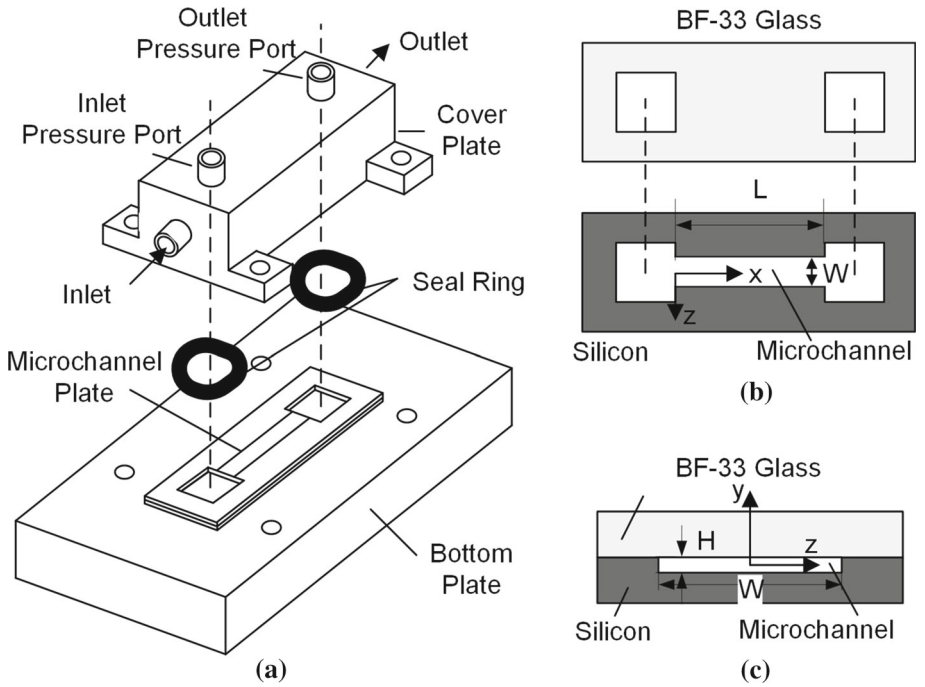

Fig. 4 Schematics of the test module: **a** exploded view of the test module; **b** exploded view of the microchannel plate; **c** cross section of the microchannel plate

average value was used as the reference temperature to determine the thermal properties. The mass flow rate of liquid through the microchannels was measured using the liquid mass collected per unit time on the electronic balance (OHAUS, EX324ZH) with an accuracy of 0.001 g. When the inlet pressure was stable, the flow was considered to have reached a steady state. In the steady state, the flow measurement was conducted for 2 $\sim$ 10 min. Each measurement was repeated at least two times.

A schematic representation of the pressure drop is shown in Fig. 7. The measured pressure drop across the inlet and outlet plenum is equal to the inlet pressure P_{in} minus outlet pressure P_{out}. Figure 7 shows that the measured pressure drop is the sum of hydrostatic pressure losses, bend losses, contraction and expansion losses, developing region effects, and frictional pressure drop (i.e., the pressure drop of fully developed region). The frictional pressure drop ΔP across the microchannel is calculated by [29]:

$$\Delta P = P_{\text{in}} - P_{\text{out}} - \Delta P_{\text{H1}} - \Delta P_{\text{H2}} - \frac{\rho u_{\text{m\_exp}}^2}{2}\left(2K_{90}\frac{A_{\text{ch}}^2}{A_{\text{p}}^2} + K_{\text{c}} + K_{\text{e}} + K(\infty)\right) \tag{11}$$

where ΔP_{H1} and ΔP_{H2} are the hydrostatic pressure losses; K_{90} is the bend loss coefficient at the channel inlet and outlet, and its recommended value is 1.2 [29]; A_{ch} and A_{p} are the cross-sectional areas of the microchannel and plenum, respectively; K_{c} and K_{e} represent the contraction and expansion loss coefficients due to the area changes, respectively, where in this work K_{c} is 1.07, and K_{e} is 1.0 [29]; $K(\infty)$ is the Hagenbach's factor, represents the developing region effects, in this work, $K(\infty)$ is 0.69 [29]; and $u_{\text{m\_exp}}$ is the experimental mean velocity, which can be calculated as follows:

$$u_{\text{m\_exp}} = \frac{\dot{m}_{\text{exp}}}{\rho A_{\text{ch}}} \tag{12}$$

where $\dot{m}_{\text{exp}}$ is the experimental mass flow rate.

Let $\Delta P_{\text{loss}} = \left(2K_{90}A_{\text{ch}}^2/A_{\text{p}}^2 + K_{\text{c}} + K_{\text{e}} + K(\infty)\right)\rho u_{\text{m\_exp}}^2/2$, for the cases of flow in channel No. 1 and No. 2, the ratio $\Delta P_{\text{loss}}/\Delta P$ is less than 0.05%, for the cases of flow in channel No. 3 and No. 4, the ratio is less than 1.6%. Therefore, the uncertainty caused by using Eq. (11) to estimate the frictional pressure drop ΔP is within an acceptable range.

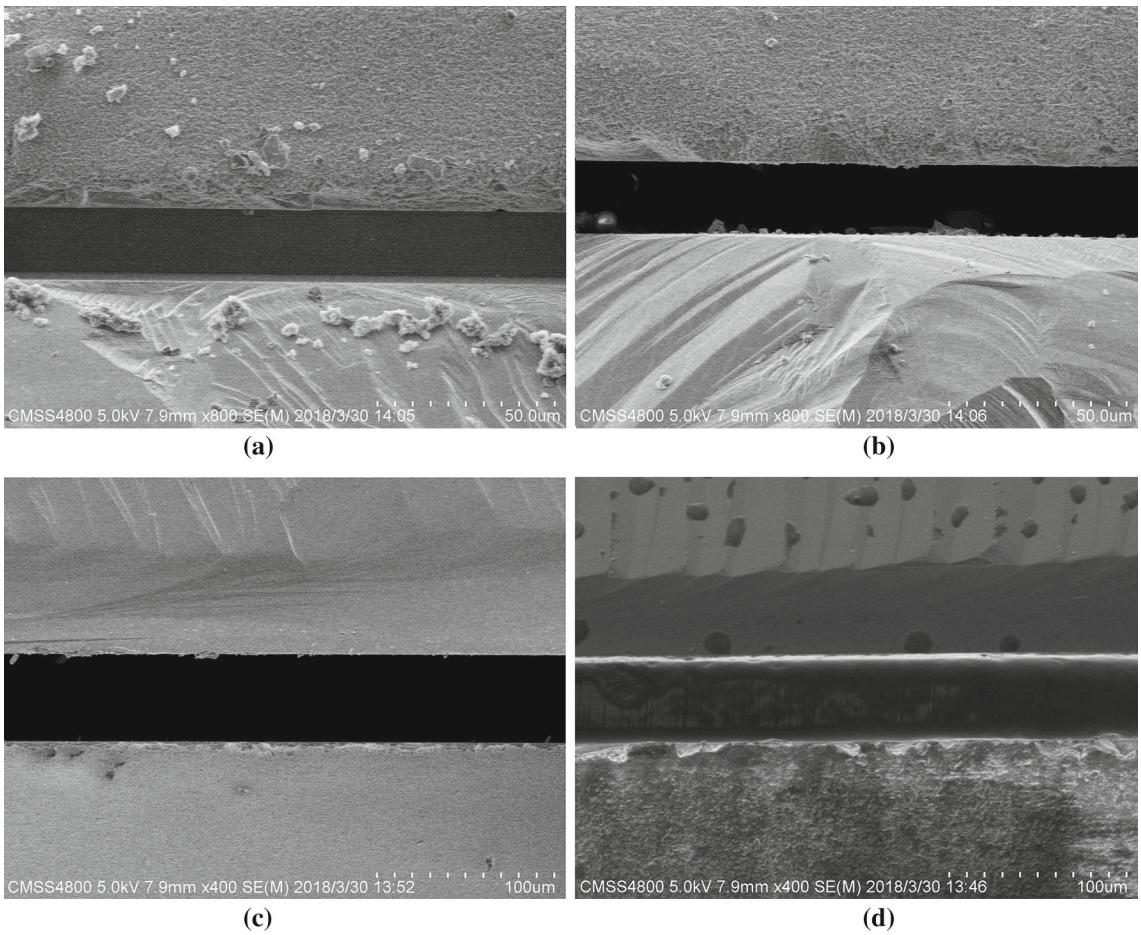

Fig. 5 SEM image of the cross section of the channel. **a** No. 1; **b** No. 2; **c** No. 3; **d** No. 4

Table 1 Dimensions of the microchannels

Channel	H (μm)	W (mm)	L (mm)
No. 1	20.3	5	25
No. 2	20.1	5	25
No. 3	50.0	5	25
No. 4	49.1	5	25

The characteristics of fluid flow can be described in terms of some dimensionless parameters, such as Reynolds number Re, Darcy's friction factor f, and Poiseuille number fRe, which can be easily related to the measured parameters as follows:

$$Re = \frac{\rho u_{\mathrm{m\_exp}} D_{\mathrm{h}}}{\mu_0}, \tag{13}$$

$$f_{\mathrm{exp}} = \frac{2D_{\mathrm{h}}}{\rho u_{\mathrm{m\_exp}}^2} \frac{\Delta P}{L}, \tag{14}$$

$$(fRe)_{\mathrm{exp}} = \frac{2D_{\mathrm{h}}^2}{\mu_0 u_{\mathrm{m\_exp}}} \frac{\Delta P}{L} \tag{15}$$

where D_{h} is the hydraulic diameter, for a rectangular channel, and it is represented by the following equation:

$$D_{\mathrm{h}} = \frac{2HW}{H + W}. \tag{16}$$

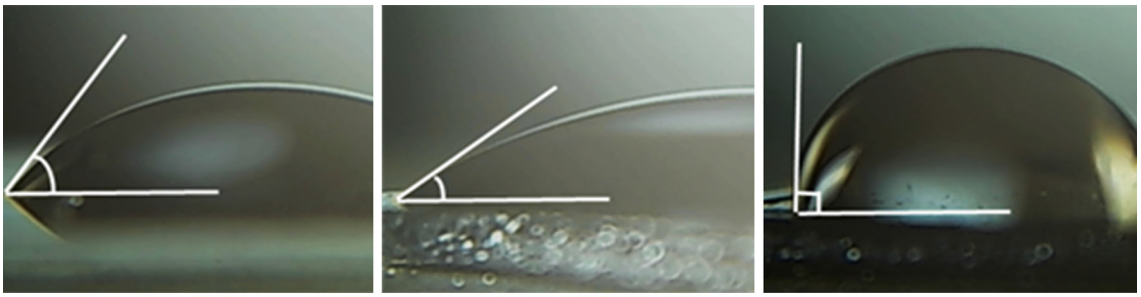

Fig. 6 Static contact angles of the interfaces: **a** top wall of all channels, BF-33 glass-water, $\theta \approx 56°$; **b** bottom wall of channels No. 1 and No. 3, silicon–water, $\theta \approx 34°$; **c** bottom wall of channels No. 2 and No. 4, silver–water, $\theta \approx 90°$

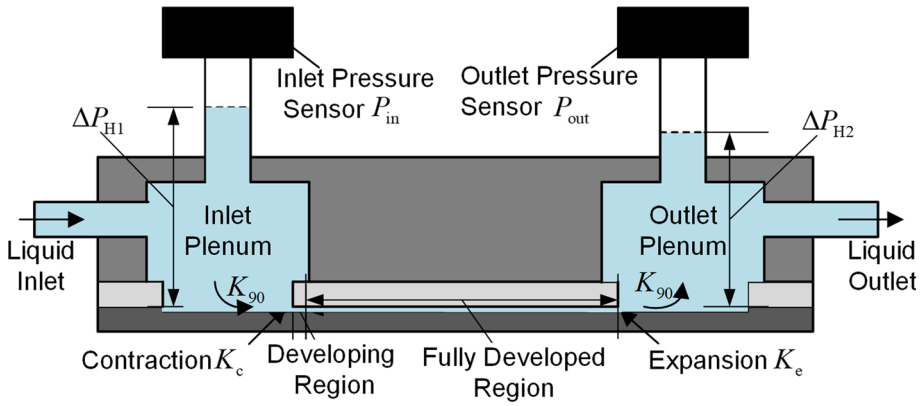

Fig. 7 Schematic of the pressure drop components

For fully developed laminar flow in a rectangular channel, the classical theoretical Poiseuille number is calculated by [30]

$$(fRe)_{\text{th}} = 96\frac{H^2 + W^2}{(H + W)^2}. \tag{17}$$

The experimental uncertainty of the parameters can be estimated by the following equation:

$$\begin{aligned} y &= f(x_1, x_2, \ldots, x_n) \\ \frac{\delta_y}{y} &= \sqrt{\left(\frac{\partial \ln f}{\partial x_1}\right)^2 \delta_{x_1}^2 + \left(\frac{\partial \ln f}{\partial x_2}\right)^2 \delta_{x_2}^2 + \cdots + \left(\frac{\partial \ln f}{\partial x_n}\right)^2 \delta_{x_n}^2} \end{aligned} \tag{18}$$

where y is a function of $x_1, x_2, \ldots x_n$, and δ is the absolute error.

4 Results and discussion

To analyze the effect of the interface wettability on the liquid microscale flow, the experimental friction factor f_{exp} and the classical theoretical value f_{th} are compared and shown in Fig. 8. f_{th} is calculated using Eq. (17).

The relative deviation Rd between f_{exp} and f_{th} is defined as

$$\text{Rd} = \frac{f_{\text{exp}} - f_{\text{th}}}{f_{\text{th}}} \times 100\%. \tag{19}$$

Figure 8 clearly shows that the trend of the experimental friction factor with Reynolds number is consistent with the laminar flow theory, which indicates that the liquid flow in the microchannel is a stable laminar flow. Figure 8a shows that the experimental friction factors are higher than the theoretical values, and such deviation

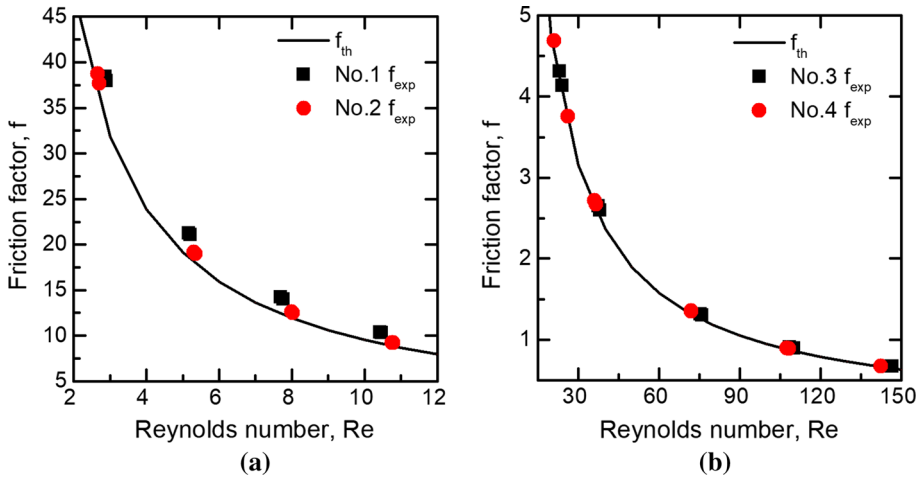

Fig. 8 Experimental friction factors versus Reynolds number and comparison with the classical theoretical values. **a** $H \approx 20\,\mu m$; **b** $H \approx 50\,\mu m$

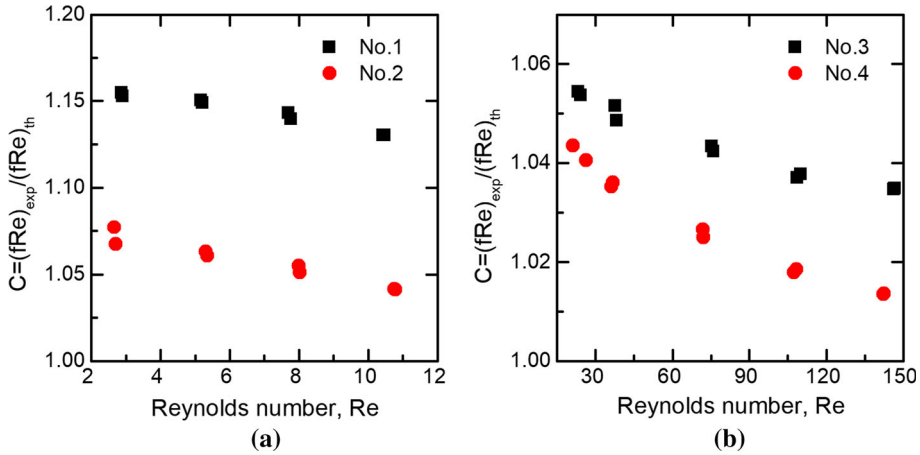

Fig. 9 Ratio of the experimental Poiseuille number to the theoretical value versus Reynolds number

decreases with the increasing pressure drop. In addition, the difference between experiment and classical theory for channel No. 1 is significantly larger than that for channel No. 2 because channel No. 1 has a stronger wettability than channel No. 2 has. According to the modified apparent viscosity model, the apparent viscosity of water increases with the increasing wettability, so the effect of the variable apparent viscosity on the flow in channel No. 1 is stronger than that in channel No. 2. The modified theory and experimental results confirm that a stronger wettability corresponds to a larger deviation between experiment and classical theory. In Fig. 8b, the experimental values are basically consistent with the theoretical values, where all relative deviations Rd are in the range of 5.4%. The uncertainties of f_{exp} estimated by Eqs. (14) and (18) are less than 1.2%, which cannot fully clarify the deviation, so the effect of the wettability on the flow remains. Comparing Fig. 8a, b, we find that the effect of the wettability on the flow decreases with increasing hydraulic diameter of the microchannel.

Figure 9 depicts the relationships between the ratio of the experimental Poiseuille number to the theoretical value and the Reynolds number. In Fig. 9, there are apparent differences in different cases; the wettability and hydraulic diameter of the microchannel significantly affect the microscale flow. For a given microchannel, the value of the ratio decreases as the pressure drop increases. This effect is because when the shear stress increases with the pressure gradient, the relative importance of the solid–liquid intermolecular force weakens with respect to the shear stress, which increases the disorder of the molecular arrangement and reduces the apparent viscosity. Liu and Pang [31] also indicated that the apparent viscosity gradually decreased with the increasing drive pressure.

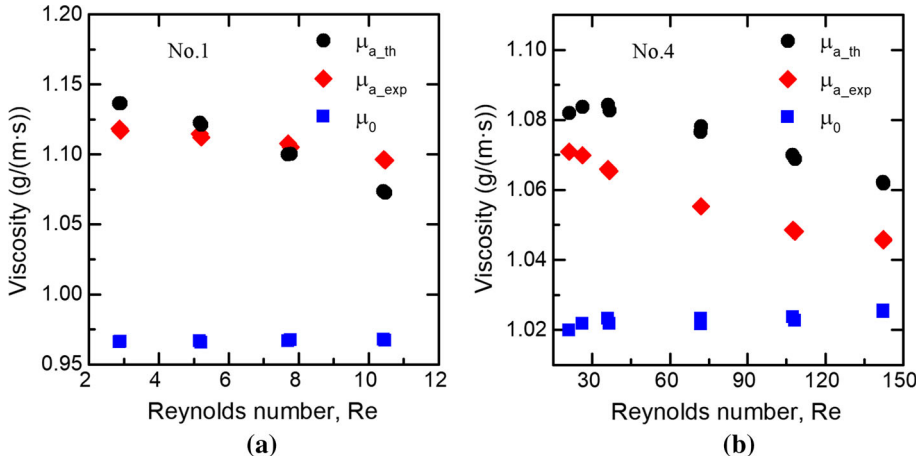

Fig. 10 Validation of the apparent viscosity model for different microchannels: **a** channel No. 1; **b** channel No. 4

To validate the modified apparent viscosity model, first, we must determine the coefficients k and n in the model. According to Eq. (8), k for each surface can be calculated by its contact angle. However, there is no exact analytical expression to calculate n. n can be estimated by substituting the experimentally determined average apparent viscosity into Eq. (9).

The experimentally determined average apparent viscosity can be calculated by

$$\bar{\mu}_{\mathrm{a\_exp}} = \frac{\rho W H^3 \Delta P}{12 \dot{m}_{\mathrm{exp}} L}. \tag{20}$$

For channel No. 2, $k_1 = \cos 56^\circ \approx 0.56$, $k_2 = \cos 90^\circ = 0$, and the effect of the bottom wall of the microchannel on the apparent viscosity can be ignored; we can obtain n_1 by combining Eqs. (20) and (9) with $\delta = 0.31$ nm for water. The value of n_1 can be fitted as a function of the pressure gradient:

$$n_1 = 8.66681 \times 10^{-4} (\Delta P/L)^2 - 3.73052 \times 10^{-4} \Delta P/L + 0.20374 \tag{21}$$

where the unit of $\Delta P/L$ is MPa/m.

Since the value of n is independent of the channel size and depends on the properties of the liquid and solid wall, Eq. (21) is also applicable to other channels with an identical solid wall, such as channel No. 4. Meanwhile, the property of the liquid plays a major role in determining n; the effect of different solid walls on n is relatively small, so we can assume that $n_2 = n_1$ for a channel with a different solid wall, e.g., channel No. 1. Therefore, the coefficients in the modified apparent viscosity model are determined. This model can be validated by the experimental data of the water flow in channels No. 1 and No. 4, which were not used to calculate n_1.

For channel No. 4, the wettability is identical to that of channel No. 2, but the height is different; $k_1 = 0.56$, $k_2 = 0$, and n_1 can be calculated using Eq. (21). For channel No. 1, the height is the same as that of channel No. 2, but the wettability is different; $k_1 = 0.56$, $k_2 = \cos 34^\circ \approx 0.83$, n_1 can be calculated by Eq. (21), assuming that $n_2 = n_1$. Then, $\bar{\mu}_{\mathrm{a}}$ at various pressure gradients for channels No. 1 and No. 4 can be calculated using Eq. (9). The bulk viscosity μ_0 of the water, the experimentally determined viscosity $\mu_{\mathrm{a\_exp}}$, and the theoretical apparent viscosity $\mu_{\mathrm{a\_th}}$ estimated by Eq. (9) are compared in Fig. 10. As shown in Fig. 10, the results of the theoretical estimation are consistent with the experimental results with a relative difference of less than $\pm$ 2.1%, which indicates that the modified apparent viscosity model is valid. The consistency between the experiment and the modified apparent viscosity model for channel No. 1 implies that the assumption $n_2 = n_1$ is valid, i.e., the property of the liquid is the decisive factor that affects the value of n. Therefore, when coefficients k and n are determined, the flow equation modified by the apparent viscosity model can be determined and accurately predict the flow of the liquid in smooth microchannels.

5 Conclusions

In this paper, the effect of the interface wettability on the apparent viscosity and liquid flow in smooth microchannels is investigated. A modified apparent viscosity model to explain the deviation between the classical theory and the experiment is proposed based on the molecular theory and wetting theory. Because of the effects of the solid–liquid interaction, the apparent viscosity of the liquid is a variable related to the distance from the wall. The apparent viscosity of the liquid is positively correlated with the interface wettability and negatively correlated with the drive pressure. The correctness of the modified apparent viscosity model is verified by the flow experiments of water in smooth parallel-plate microchannels with different wettabilities. The experimental results show that the friction factor is higher than that predicted by the classical theory. This relative deviation increases with increasing wettability and decreases with increasing hydraulic diameter and drive pressure. The coefficients in the apparent viscosity model can be determined using the experimental data of channel No. 2 and the contact angles. The apparent viscosity calculated by the apparent viscosity model is consistent with the experimental results. Thus, the flow equation modified by the apparent viscosity model can accurately predict the laminar flow behavior of a liquid in a smooth microchannel. The modified model and experimental design proposed in this investigation provide us with a deep understanding of the flow characteristics in microchannels and are helpful for the improvement of microfluidic devices.

Acknowledgements This work was supported by the National Natural Science Foundation of China (No. 11702320) and the Training Program of the Major Research Plan of the National Natural Science Foundation of China (No. 91741107).

References

1. Ho, C.M., Tai, Y.C.: Micro-electro-mechanical-systems (MEMS) and fluid flows. Ann. Rev. Fluid Mech. **30**, 579–612 (1998)
2. Stone, H.A., Stroock, A., Ajdari, A.: Engineering flows in small devices: microfluidics toward a lab-on-a-chip. Ann. Rev. Fluid Mech. **36**, 381–411 (2004)
3. Peng, X.F., Peterson, G.P., Wang, B.X.: Heat transfer characteristics of water flowing through microchannels. Exp. Heat Transf. **7**, 265–283 (1994)
4. Qu, W.L., Mala, G.M., Li, D.Q.: Pressure-driven water flows in trapezoidal silicon microchannels. Int. J. Heat Mass Transf. **43**, 353–364 (2000)
5. Zhigang, L., Ning, G., Chengwu, Z., Xiaobao, Z.: Experimental study on flow and heat transfer in a 19.6-μm microtube. Exp. Heat Transf. **22**, 178–197 (2009)
6. Li, Z.X., Du, D.X., Guo, Z.Y.: Experimental study on flow characteristics of liquid in circular microtubes. Microscale Thermophys. Eng. **7**, 253–265 (2003)
7. Peng, X.F., Peterson, G.P., Wang, B.X.: Frictional flow characteristics of water flowing through microchannels. Exp. Heat Transf. **7**, 249–264 (1994)
8. Mala, G.M., Li, D.Q.: Flow characteristics of water in microtubes. Int. J. Heat Fluid Flow **20**, 142–148 (1999)
9. Liu, Y.P., Xu, G.Q., Sun, J.N., Li, H.W.: Investigation of the roughness effect on flow behavior and heat transfer characteristics in microchannels. Int. J. Heat Mass Transf. **83**, 11–20 (2015)
10. Kandlikar, S.G., Joshi, S., Tian, S.: Effect of surface roughness on heat transfer and fluid flow characteristics at low Reynolds numbers in small diameter tubes. Heat Transf. Eng. **24**, 4–16 (2003)
11. Choi, C.H., Westin, K.J.A., Breuer, K.S.: Apparent slip in hydrophilic and hydrophobic microchannels. Phys. Fluids **15**, 2897–2902 (2003)
12. Nagayama, G., Matsumoto, T., Fukushima, K., Tsuruta, T.: Scale effect of slip boundary condition at solid–liquid interface. Sci. Rep. **7**, 43125 (2017)
13. Wang, F., Yue, X.A., Xu, S.L., Zhang, L.J., Zhao, R.B., Hou, J.R.: Influence of wettability on flow characteristics of water through microtubes and cores. Chin. Sci. Bull. **54**, 2256–2262 (2009)
14. Nagayama, G., Cheng, P.: Effects of interface wettability on microscale flow by molecular dynamics simulation. Int. J. Heat Mass Transf. **47**, 501–513 (2004)
15. Mala, G.M., Li, D.Q., Werner, C., Jacobasch, H.J., Ning, Y.B.: Flow characteristics of water through a microchannel between two parallel plates with electrokinetic effects. Int. J. Heat Fluid Flow **18**, 489–496 (1997)
16. Ren, L.Q., Qu, W.L., Li, D.Q.: Interfacial electrokinetic effects on liquid flow in microchannels. Int. J. Heat Mass Transf. **44**, 3125–3134 (2001)
17. Xu, S.L., Yue, X.A., Hou, J.R.: Experimental investigation on flow characteristics of deionized water in microtubes. Chin. Sci. Bull. **52**, 849–854 (2007)
18. You, X.Y., Zheng, J.R., Jing, Q.: Effects of boundary slip and apparent viscosity on the stability of microchannel flow. Forsch. Ing. Wes. **71**, 99–106 (2007)
19. Mala, G.M., Li, D.Q., Dale, J.D.: Heat transfer and fluid flow in microchannels. Int. J. Heat Mass Transf. **40**, 3079–3088 (1997)
20. Israelachvili, J.N.: Measurement of the viscosity of liquids in very thin films. J. Colloid Interface Sci. **110**, 263–271 (1986)
21. Gee, M.L., Mcguiggan, P.M., Israelachvili, J.N., Homola, A.M.: Liquid to solidlike transitions of molecularly thin films under shear. J. Chem. Phys. **93**, 1895–1906 (1990)

22. Lv, P., Yang, Z.H., Hua, Z., Li, M.Y., Lin, M.Q., Dong, Z.X.: Viscosity of water and hydrocarbon changes with micro-crevice thickness. Colloids Surf. A Physicochem. Eng. Asp. **504**, 287–297 (2016)
23. Thomas, J.A., Mcgaughey, A.J.H.: Reassessing fast water transport through carbon nanotubes. Nano Lett. **8**, 2788–2793 (2008)
24. Suk, M.E., Aluru, N.R.: Molecular and continuum hydrodynamics in graphene nanopores. RSC Adv. **3**, 9365–9372 (2013)
25. Ghorbanian, J., Beskok, A.: Scale effects in nano-channel liquid flows. Microfluid. Nanofluid. **20**, 121 (2016)
26. Blake, T.D., Coninck, J.D.: The influence of solid–liquid interactions on dynamic wetting. Adv. Colloid Interface Sci. **96**, 21–36 (2002)
27. Zhang, F.T.: Interface layer model of physical interface. J. Colloid Interface Sci. **244**, 271–281 (2001)
28. Tretheway, D.C., Meinhart, C.D.: Apparent fluid slip at hydrophobic microchannel walls. Phys. Fluids **14**, 9–12 (2002)
29. Kandlikar, S.G., Garimella, S., Li, D.Q., Colin, S., King, M.R.: Heat Transfer and Fluid Flow in Minichannels and Microchannels. Elsevier Ltd, Oxford (2006)
30. Dey, R., Das, T., Chakraborty, S.: Frictional and heat transfer characteristics of single-phase microchannel liquid flows. Heat Transf. Eng. **33**, 425–446 (2012)
31. Liu, Z.M., Pang, Y.: Effect of the size and pressure on the modified viscosity of water in microchannels. Acta Mech. Sin. **31**, 45–52 (2015)